AIAA 80-0436R

High-Resolution LDA Measurements of Reynolds Stress in Boundary Layers and Wakes

Kenneth L. Orloff* and Lawrence E. Olson*
NASA Ames Research Center, Moffet Field, Calif.

The turbulent character of the boundary layer and wake associated with an airfoil has been studied at a Reynolds number of 10^6 and a Mach number of 0.1. To accomplish these measurements, a unique laser Doppler anemometer (LDA) has been developed that is capable of sensing two velocity components from a remote distance of 2.13 m. Using special simultaneity logic and counter-type signal processors, the geometrical features of the LDA have been exploited to provide variable spatial resolution as low as 0.2 mm. By combining the LDA with an on-line computerized data acquisition and display system, it has been possible to measure mean velocity and Reynolds stress tensor distribution at several locations along the upper surface of a 0.9 m chord, flapped airfoil installed in the Ames 7-by 10-Foot Wind Tunnel.

Introduction

THE laser Doppler anemometer (LDA) provides an ideal means for the remote, nonintrusive measurement of complex aerodynamic flows. Generally, LDA studies of wake, jet, and boundary-layer flows are conducted in relatively small facilities that are compatible with the range and spatial resolution capabilities of the LDA optical system. In the case of research on multielement airfoils, it is desirable to study the associated boundary layers and wakes on a scale large enough to generate viscous regions of adequate thickness to probe experimentally and to yield a high Reynolds number at low Mach number to correctly simulate a high-lift, slow-speed condition.

Although LDA operation in wind-tunnel facilities has become relatively routine for remote sensing at distances in excess of several meters,[1] the dual requirements of long-range remote sensing and spatial resolution fine enough to adequately probe boundary layers and thin wakes are mutually conflicting (in an optical sense) for conventional LDA instruments. This paper describes a unique LDA that has been developed to overcome this problem. The instrument is capable of sensing two velocity components with a spatial resolution of better than 0.2 mm from a remote distance of 2.13 m.

In addition to optical considerations, the procedures used for signal processing and data acquisition are also critical to the accurate measurement of the parameters generally used to statistically characterize a turbulent flow. For incompressible flow that is "in the mean" two-dimensional, the parameters of primary interest are the three nonzero terms of the Reynolds stress tensor, $\overline{u'^2}$, $\overline{v'^2}$, and $\overline{u'v'}$. For the two-dimensional case, it has been demonstrated[2,3] that a single velocity component LDA can be used to determine Reynolds stress. However, the experimental technique described in Refs. 2 and 3 does not make a direct measurement of the cross correlation component $\overline{u'v'}$ of the stress tensor. Instead, the cross-correlation is obtained from measurements of the mean-square fluctuations of two velocity components that are ± 45 deg relative to the direction of the mean flow, $\bar{u}$. Recognizing the additional versatility and utility of the modern two-channel LDA instrument, a more desirable experimental approach for determining the Reynolds shear stress is to cross-correlate the two velocity components directly. For discretely sampled data, this can be done either by 1) collecting data from each channel along with the arrival time of each sample and then computing the correlation in the subsequent data reduction[4] or 2) by using timing logic to designate simultaneous velocity pair values (u,v) and collecting an ensemble of these pairs. While the former method requires precise timing information and considerable data storage capability, it is attractive when the turbulent power spectrum is also to be measured. The ensemble method, which requires less data and no timing information other than simultaneity, has been selected to be used with the LDA described here.

Unlike other LDA instruments, the geometrical arrangement of this optical system and the timing logic are related in such a way as to enhance the spatial resolution. The LDA was combined with counter-type signal processors, simultaneity logic, and a user-interactive computerized data acquisition, data reduction, and data display system. Results are reported here on the application of the LDA to the measurement of the turbulent structure within the boundary layers, wakes, and confluent boundary layer on a 0.9 m chord, two-element airfoil installed in the Ames 7-by 10-Foot Wind Tunnel.

High-Resolution LDA

Optical Design Considerations

The high-resolution LDA instrument developed for this investigation is shown in Fig. 1. Two velocity components are sensed by utilizing two distinct output colors (514.5 and 488.0 nm wavelength) of an argon-ion laser. Using three dense flint dispersion prisms in series, followed by a special separator prism, the two colors are efficiently separated from the "all-lines" laser output. A series of mirrors then directs each color into a beamsplitter followed by an acousto-optic cell (to remove directional ambiguity). To maintain coherence and ensure a sharp interference pattern within the probe volume at the beam crossover, either of two methods can be used: 1) an intercavity etalon can be installed within the laser (the configuration shown in Fig. 1) or 2) an additional mirror can be used after the acousto-optic cell to equalize path length by increasing the path length of the beam in each pair that travels the shorter distance to the telescope. The latter method was eventually selected due to the difficulty of achieving broadband operation of the etalon at total light power levels in excess of 800 mW.

Submitted March 3, 1980; presented as Paper 80-0436 at the AIAA 11th Aerodynamic Testing Conference, Colorado Springs, Colo., March 18-20, 1980; revision received Sept. 18, 1981. This paper is declared a work of the U. S. Government and therefore is in the public domain.

*Aerospace Engineer. Member AIAA.

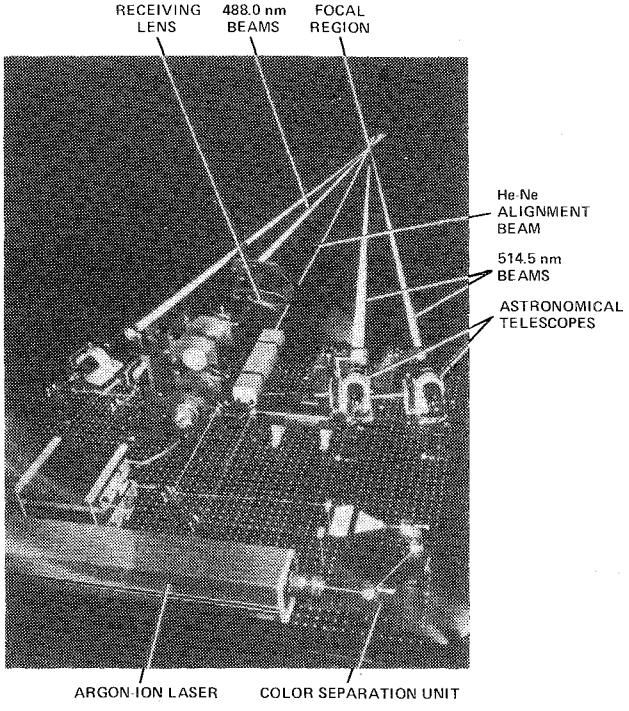

Fig. 1 Two-velocity-component LDA designed for a spatial resolution of 0.2 mm at a distance of 2.13 m).

Whereas conventional LDA optical units direct the parallel beams through a common focusing lens to form the cross-beam arrangement of a dual-scatter LDA, a key feature of this high-resolution LDA is the use of expansion telescopes to enlarge each 3-mm-diam beam to 50-mm-diam before focusing them into the flowfield. The telescopes utilized are of the astronomical refracting type with 8-μm-diam spatial filters, thus generating output beams having a smooth Gaussian intensity profile. Expansion of the output beams to 50 mm before focusing is used to improve spatial resolution by reducing the waist dimension of each focused beam at the crosspoint. The focusing lenses have a focal length of approximately 2 m; hence the f-number is large, and diffraction-limited operation can be realized. The diffraction-limited spot size (waist diameter) for each beam is calculated to be 53 μm although the measured size is closer to 60 μm. These output beams form two LDA dual-scatter patterns that are not orthogonal, but rather separated by approximately 25 deg so as to define nonorthogonal velocity components.

A 1-mW helium-neon laser beam (3-mm-diam at the crosspoint) is used for alignment purposes. It defines the optical centerline of the instrument and is parallel to the direction of motion of the entire optical package.

The light receiving part of the LDA, also shown in Fig. 1, is of the backscatter variety. Because the focused spot sizes are small, the light energy density at the crosspoint is high. As a result, the required laser power was significantly below that which would otherwise have been required for an LDA operating in the backscatter mode at a range of over 2 m. Under test operating conditions, at an indicated total power output of 900 mW, each 488.0-nm output beam was measured to be 50 mW and each 514.5-nm output beam was measured to be 30 mW. The 100-mm aperture receiving lens collects scattered light 10 deg off-axis above the optical centerline, serving to further reduce the effective size of the probe volume. After dichroic color separation of the collected light, the focused images of the 488.0- and 514.5-nm probe volumes are received by the upper and lower photomultiplier tubes, respectively, as shown in Fig. 1. Spatial filtering is accomplished with 125-μm apertures attached to each photodetector and positioned in the image plane of the receiving lens; this restricts the optical field of view to a circular region 250 μm in diameter and nearly normal to the optical centerline. The spatial filtering is necessary to reject off-centerline light that can generate high noise levels, especially when measurements are made within a boundary layer and when the optical centerline is normal to the surface of the airfoil. However, when the distance from the focal volume to the surface is less than a few centimeters, this spatial filtering is no longer adequate to effect the required light rejection. Hence, a high-reflectance dielectric mirror is imbedded in the surface of the airfoil to minimize light flare. By use of this technique, it has been possible to obtain processable signals from the photodetectors with the probe volume positioned within 0.5 mm of the surface.

Optical Alignment Procedures

A measurement of the $\overline{u'v'}$ component of the Reynolds stress tensor at a point within the shear flow requires that each channel of the LDA generate nearly *simultaneous* velocity measurements. Because of the small size of the probe volume and the density of the scattering particles in the wind tunnel,† this requirement translates into the constraint that both channels of the LDA detect the *same* particle nearly simultaneously. Figure 2a is a sketch of the beam crossover region showing two possible particle trajectories (A and B) that pass through the interference (fringe) regions of each channel but on opposite sides of the central crossover point. For a given particle, exact simultaneity can occur only if 1) the minimum beam waist portion of all four focused laser beams overlap precisely and 2) if the particle's trajectory takes it through the exact center of this overlap region.

In addition to increasing the waist size at the crossover point, Durst and Stevenson[5] have shown that failure to correct for the divergence of the laser output beam can introduce errors in fringe spacing. In this LDA system, however, it is possible to attain nearly diffraction-limited performance and to maintain a uniform fringe spacing by decollimating the expansion telescopes so as to position the smallest beam waist at the crossover point of all beams.

The instrument is aligned by positioning a 50-μm aperture normal to the helium-neon laser beam at a distance of 2.13 m. The aperture is visually set approximately at the center of this beam. In-plane adjustments are then made of the focusing lenses to make all four beams pass through the aperture; this is best accomplished by viewing the circular aperture diffraction pattern projected on a screen set behind the aperture.

To simulate particle passage, a 5-μm-diam wire extending approximately 4 mm radially from the edge of a spinning disk is passed repeatedly (53.3 times/s) through the center of the overlap region; when passing through the focal volume, the axis of the wire is normal to the optical centerline (Fig. 2). The resulting burst signals from the two LDA channels are monitored on a dual-trace oscilloscope. Examples of these traces are presented in Fig. 2b. At a wire speed of 26.8 m/s, a time "jitter" of approximately 0.5 μs is noted in the time interval between the arrival of the two signal bursts; this jitter occurs because the wire is not rigid and hence there is some uncertainty in the location of the wire along the optical centerline within the probe volume.

During the alignment procedure, the wire is traversed along the optical axis until simultaneous signals (within the time jitter) are observed on the oscilloscope. The 125-μm aperture at each phototube is then positioned so as to yield a maximum data rate from the processing electronics. At this point, the LDA is aligned and is ready to be used on the flowfield of interest.

To keep the LDA in alignment, it is important that 1) each expansion telescope (with 8-μm spatial filter) remain precisely

†Mineral oil aerosol of nominally 2-μm diam is introduced into the diffuser section of the (closed-circuit) wind tunnel to produce nearly uniform seeding of the test section.

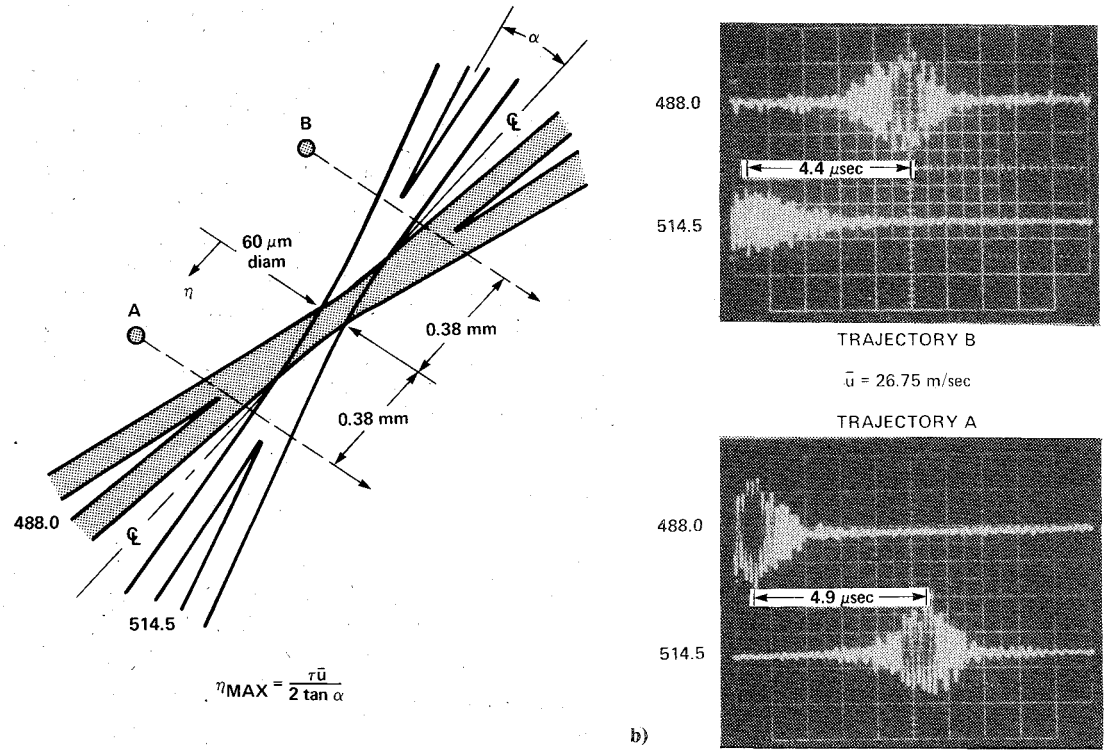

Fig. 2 Scattering volume and characteristic Doppler bursts: a) crossover region showing two possible particle trajectories through the interference (fringe) regions of each LDA channel; b) burst signals (from wire simulation) for each LDA channel, corresponding to trajectories A and B, showing temporal separation due to LDA geometry.

positioned with respect to one another and relative to all other optical components, 2) exact overlap of all four 60-μm-diam focused beams be maintained, and 3) the location of the 125-μm-diam phototube apertures remain constant relative to all other optical components. To satisfy these requirements, the ambient temperature in the environment surrounding the LDA must be held nearly constant. The linear coefficient of thermal expansion for the optical platform (to which all components are attached) is 10.4 μm/m/°C. Based on this value, an estimated maximum tolerable dimensional distortion of ± 30 μm for the LDA platform will result if the ambient temperature is not constant to within ± 2°C. This estimate is in agreement with the actual performance of the LDA during the wind-tunnel test where it was also observed that gradual ambient temperature changes in excess of ± 2°C could not be tolerated.

Simultaneity

Simultaneity of the detected signal bursts is most likely to occur if the 488.0- and 514.5-nm focal volumes cross symmetrically as shown in Fig. 2a. In order for the LDA to perform correctly, not only must the two beams of each channel overlap accurately, but the focal volumes for the two channels themselves must also overlap accurately. The precision with which this overlap has been attained by the optical alignment procedure can be quantified by noting the signal processing rate of each LDA channel as a function of position along the optical axis (using the 5-μm wire on the rotating disk as a target). Normalization of these rates by the maximum data rate possible (53.3/s) yields the detection probability. Figure 3 presents the variation of this probability along the optical centerline; the results confirm that the desired overlap and symmetry have been attained. This information can also be used to specify the spatial resolution for each LDA channel as the width of the distribution at 1/e of the maximum. Since the respective widths for the two channels are nearly the same, the single-channel spatial resolution is taken to be 1.0 mm. The maximum measured

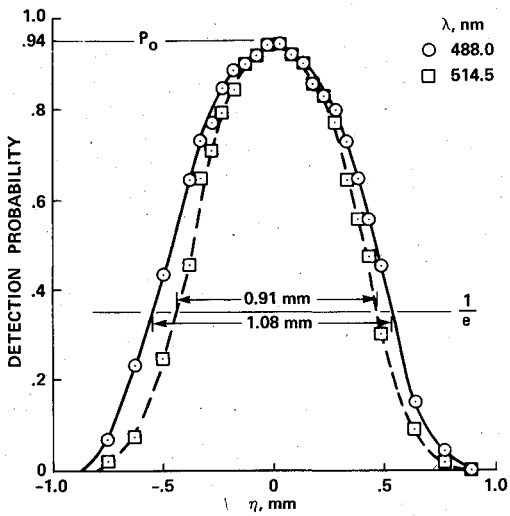

Fig. 3 Spatial resolution for each LDA channel separately as determined from wire simulation (η is coordinate measured from the crossover center, as indicated in Fig. 2a).

probability of $P_0 = 0.94$ suggests that some of the burst signals result in a low signal/noise level (not uncommon for backscatter LDA) or poor signal periodicity; hence, either they do not produce the required number of cycles for processing or they are rejected (based on periodicity) by the processor logic, respectively.

Because the axes of the two LDA channels are at an angle to one another (approximately 25 deg for this system), the burst signal detected in one channel may not be exactly coincident with the other channel when a particle's path is slightly displaced from the central crossover point (see example in Fig. 2). It is possible to exploit this geometrical feature of the LDA to further improve the spatial resolution. By selecting the width τ of the simultaneity interval (typically 1-20 μs), the

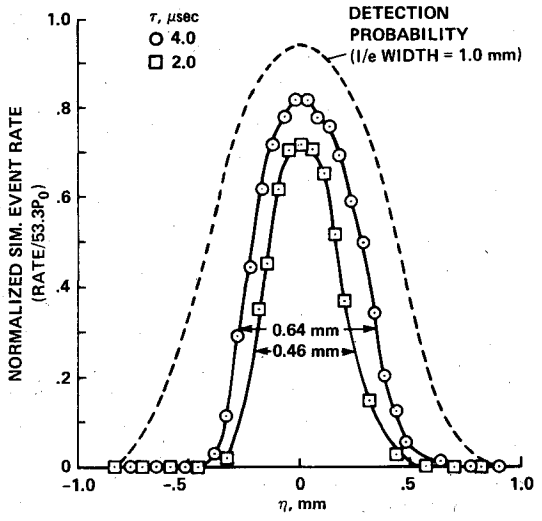

Fig. 4 Normalized simultaneity event rate measured along the optical centerline to demonstrate improved spatial resolution; single-channel detection probability is shown for comparison.

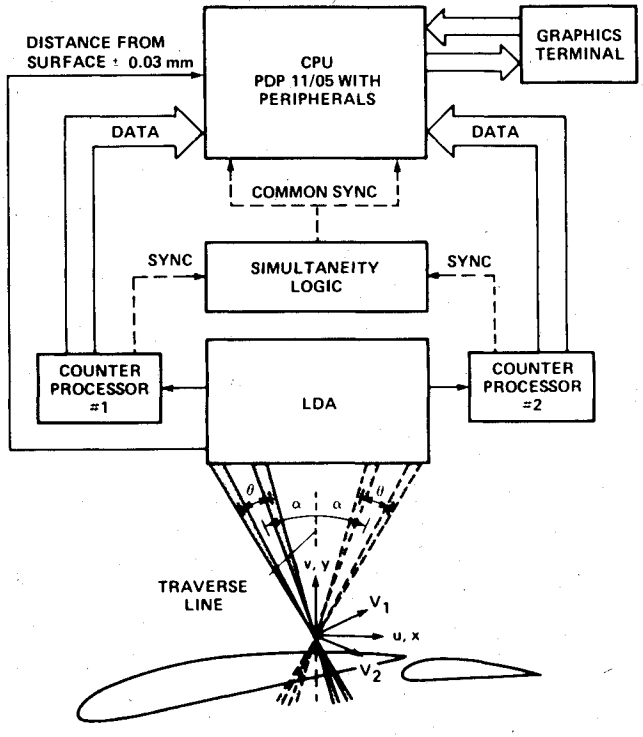

Fig. 5 Data management system used for LDA Reynolds stress measurements (indicated are the simultaneity timing logic, data acquisition system, two-element airfoil, and the manner in which the LDA beams define the velocity components and angles).

spatial resolution can be expressed as

$$\eta_{max} = \tau\bar{u}/(2\tan\alpha) \qquad (1)$$

where $\bar{u}$ is the mean velocity normal to the optical centerline, η_{max} the maximum distance along the centerline away from the crossover that a particle can traverse and still meet the simultaneity criterion, and α the angle between the bisector of either beam pair and the optical centerline. A data pair (one processed signal from each LDA channel) is considered to be acceptable only if the interarrival time is less than τ. In regions of high mean shear, τ can be selected to yield a spatial resolution as small as 0.2 mm. In regions of low mean shear, the simultaneity requirement can be relaxed to maximize the data rate without compromising the quality of the data.

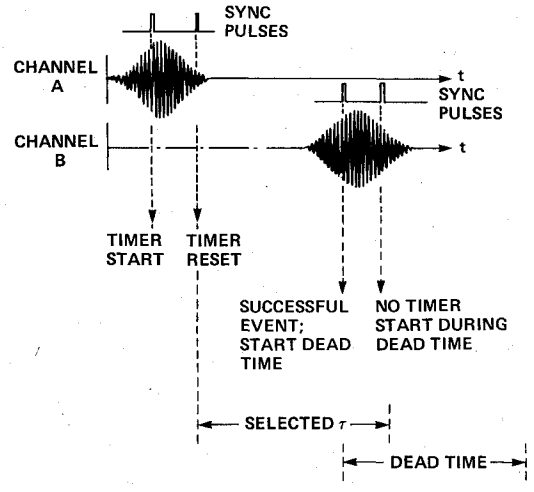

Fig. 6 Timing logic used to determine simultaneous events.

The variation in the simultaneity event rate (SER) through the crossover region can be measured by using the 5-μm wire to generate simulated flow data. Figure 4 presents the normalized SER for two selected simultaneity intervals that are appropriate for the wire speed of 26.75 m/s; the detection probability curve for a spatial resolution of 1.0 mm is also shown for comparison. By rejecting all data pairs with interarrival times greater than the selected value, the spatial resolution of the LDA is significantly improved. For time intervals of 4.0 and 2.0 μs, the measured resolutions are 0.64 and 0.46 mm, respectively (1/e widths). Equation (1) predicts respective values of 0.49 and 0.25 mm. The larger measured values are attributed to the time jitter due to fluctuations in the wire position and to a lack of knowledge as to the exact location within the fringe region where the processing takes place. The latter influence will be less pronounced when the selected time interval is much longer than the signal burst time. As indicated in Fig. 2b, the burst times in this simulation are comparable with the selected time intervals.

Data Management

Data Acquisition and Reduction

The LDA signals are processed by counter-type signal processors. As indicated in Fig. 5, the simultaneity logic interface interrupts the "data ready" sync pulses from the processors. The interface determines if the time interval between the arrival of these pulses is less than the selected simultaneity time; if so, it initiates data transfer to the minicomputer.

The simultaneity interface timer can be started by either LDA channel (see Fig. 6). If there are enough cycles in the Doppler burst from the initiating channel, there will be more than one sync pulse; the timer is reset by each subsequent sync pulse from channel A. When a "data ready" pulse is received from the second channel (B) before the end of the selected interarrival time τ, a common sync pulse is generated to initiate data transfer to the CPU. The data are transferred into the CPU simultaneously and are indexed as a (v_1, v_2) velocity pair. Additionally, a dead time period is begun during which the timer cannot be restarted to provide protection against the possibility that the same particle is used for more than one data pair; the importance of this has been discussed by Meyers.[6]

A stepping motor attached to a ballscrew-ballnut arrangement is used to position the LDA optical system. The location of the probe volume center is read directly into the CPU from a counter-readout unit that is incremented by an optical shaft-angle encoder; this value is accurate to within ±0.03 mm (based on backlash and stepping accuracy).

	MEAN VELOCITIES, m/sec		REYNOLDS STRESSES, m^2/sec^2		
	PARALLEL, $\bar{u}$	NORMAL, $\bar{v}$	$\overline{u'^2}$	$\overline{v'^2}$	$-\overline{u'v'}$
ARITHMETIC AVERAGE	18.85	3.29	1.73	4.06	-0.356
VELOCITY-WEIGHTED AVERAGE	18.75	3.24	1.79	3.99	-0.384
RESIDENCE TIME CORRECTION	0.5%	1.5%	3.4%	1.8%	7.3%

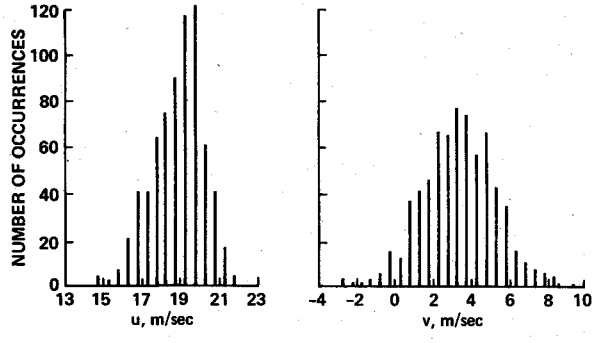

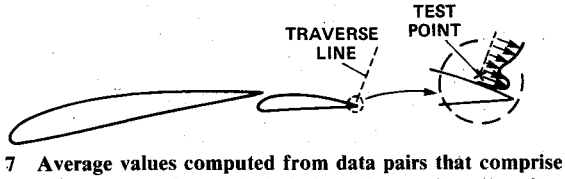

Fig. 7 Average values computed from data pairs that comprise the velocity histograms shown (tabulation shows the necessity for residence time biasing corrections).

During data acquisition, the CPU collects data pairs, calculates velocities v_1 and v_2 in nonorthogonal LDA coordinates (Fig. 5), and displays the developing histograms (velocity probability) for these velocities on the graphics terminal. After a user-selectable number of pairs N are collected for a point along the traverse line, a data-editing program eliminates data pairs for which either v_1 or v_2 are more than three standard deviations from the mean values $\bar{v}_1$ and $\bar{v}_2$, respectively. For highly-skewed distributions this procedure may not be entirely valid and caution must be exercised to insure that the editing process does not itself introduce a biasing error. Nevertheless, for nearly normal distributions the procedure is an effective means for removing questionable data that may have resulted from erroneous signal processings. The remaining data pairs are transformed to orthogonal coordinates according to

$$u=(v_1+v_2)/(2\cos\alpha) \qquad v=(v_1-v_2)/(2\sin\alpha) \tag{2}$$

with

$$v_1=\frac{\lambda_1(f_1-f_1^0)}{2\sin(\theta/2)}; \qquad v_2=\frac{\lambda_2(f_2-f_2^0)}{2\sin(\theta/2)} \tag{3}$$

where $\lambda_1=0.4880\ \mu$m, $\lambda_2=0.5145\ \mu$m, f_1^0 and f_2^0 are selected offset frequencies to remove directional ambiguity, and f_1 and f_2 are frequencies of burst signals as measured by the counter processors. The velocity components defined by Eqs. (2) are parallel (u) and normal (v) to the surface of the airfoil (boundary layer) or to a streamline (wake); the alignment is accomplished by setting the He-Ne beam normal to the appropriate surface or streamline. Figure 7 presents typical histograms for the velocity components in the orthogonal coordinate system. Using these values, mean velocity, turbulence intensity, and Reynolds shear stress are computed. Velocity and Reynolds stress profiles are determined by acquiring a number of such pair ensembles along a traverse line normal to the surface (or normal to the wake streamline).

Uncertainty and Biasing Considerations

Mean velocities ($\bar{u},\bar{v}$) and the three nonzero components of the Reynolds stress tensor ($\overline{u'^2}$, $\overline{v'^2}$, and $-\overline{u'v'}$) in the boundary-layer and wake coordinate systems are computed using the ensemble values (u_i,v_i) where $i=1,\ldots,N$. From Eqs. (2) and (3), the uncertainty in u_i and v_i (at a freestream speed of 20 m/s) is calculated to be 3% and 11%, respectively. These values are based on uncertainties in the geometrical arrangement (errors in the measurement of θ and α) and the processing accuracy of the electronics. Since the components of the Reynolds stress tensor involve velocity differences, systematic errors in measuring the geometrical arrangement are expected to have the greatest influence on the mean values $\bar{u}$ and $\bar{v}$. Hence, the large systematic uncertainty in the measurement of $\bar{v}$ does not affect the precision with which the stress tensor can be measured; the percentage uncertainty in the stress tensor is determined only by the processor accuracy.

As pointed out by Buchhave et al.[7] and George,[8] as the turbulence level increases, an error known as "residence time biasing" becomes more pronounced in the ensemble averaging process; this occurs because an ensemble average is not exactly the same as the time average when using LDA data. To minimize the effect, the averaging process used here includes a two-dimensional weighting function given by

$$w_k=(u_k^2+v_k^2)^{-1/2} \tag{4}$$

for the kth pair. The weighted averages are computed from

$$\bar{u}=\sum_{i=1}^{N} w_i u_i/S \qquad \overline{u'^2}=\sum_{i=1}^{N} w_i(u_i-\bar{u})^2/S$$
$$\bar{v}=\sum_{i=1}^{N} w_i v_i/S \qquad \overline{v'^2}=\sum_{i=1}^{N} w_i(v_i-\bar{v})^2/S \tag{5}$$
$$\overline{u'v'}=\sum_{i=1}^{N} w_i(u_i-\bar{u})(v_i-\bar{v})/S$$

where

$$S=\sum_{i=1}^{N} w_i$$

Figure 7 presents both the arithmetic averages and the velocity-weighted averages for an ensemble containing $N=788$ velocity pairs. As expected for residence time biasing, the arithmetic mean velocities are higher than the weighted averages. Whereas the errors in $\bar{u}$ and $\bar{v}$ are not large, failure to use corrected mean values in the higher moments will generate even larger percentage errors in the calculated components of the Reynolds stress tensor, compounding to an error of 7.3% in the $\overline{u'v'}$ cross-correlation.

For a large number of samples, the statistics of the velocity probability distribution (histograms in Fig. 7) are nearly normal and the statistical uncertainties in the mean, variance, and covariance can be written as[9]

$$\bar{u}\pm z_c\frac{u'_{\rm rms}}{\sqrt{N}}, \qquad \overline{u'^2}\pm z_c\overline{u'^2}\sqrt{2/N}$$
$$\bar{v}\pm z_c\frac{v'_{\rm rms}}{\sqrt{N}}, \qquad \overline{v'^2}\pm z_c\overline{v'^2}\sqrt{2/N} \tag{6}$$
$$\overline{u'v'}\pm z_c\overline{u'v'}\sqrt{2/N}$$

Table 1 Uncertainty estimates ($N = 788$ samples)

	$\bar{u}$, m/s	$\bar{v}$, m/s	$\overline{u'^2}$	$\overline{v'^2}$	$-\overline{u'v'}$
Velocity-weighted average	18.75	3.24	1.79 (m/s)^2	3.99 (m/s)^2	−0.384 (m/s)^2
Combined systematic and processing uncertainty	0.6[a]	2.2[a]	1%	1%	1%
Statistical uncertainty[b]	0.09	0.14	10%	10%	10%

[a]Based on a freestream velocity of 20 m/s. [b]95% confidence level that uncertainty is less than this amount.

where z_c is the confidence coefficient for a normal distribution. Notice that the statistical uncertainty in the mean velocities is independent of the mean value and is dependent on the standard deviation (rms). Conversely, the statistical uncertainty in the components of the Reynolds stress tensor are dependent on the values themselves. Therefore, the *percentage* uncertainty is only a function of the number of samples N. Hence, it is appropriate to express the estimated statistical uncertainty as an absolute value for $\bar{u}$ and $\bar{v}$ and as a percentage value for the stress tensor components. A listing of the calculated uncertainties for the ensemble shown in Fig. 7 is given in Table 1. A 95% confidence level that the statistical uncertainty is less than the percentage shown is obtained by setting $z_c = 1.96$.

Typical Results

The high-resolution LDA has been used to study the turbulent structure within the boundary layers and wakes associated with a two-element airfoil installed in the Ames 7- by 10-Foot Wind Tunnel. The airfoil shape was similar to that depicted in Fig. 5; it consisted of a 0.9-m-chord NACA 4412 main section and a 0.36-m-chord NACA 4415 slotted flap. The flap was deflected downward 10 deg and the slot width was nominally 1.75 cm. The model angle of attack was set at 2.2 deg, resulting in a section lift coefficient of 1.9. At the test Reynolds number of 1.2×10^6 and a test Mach number of 0.6, neither airfoil element showed any detectable flow separation.

To simulate two-dimensional flow, the model spanned the wind tunnel vertically‡ and all LDA measurements were made at the midspan location. Mean velocity profiles and Reynolds stress tensor distributions were measured at four locations along the upper surface of the airfoils and two locations downstream of the flap trailing edge.

Figure 8a presents the variation of the measured component of velocity that is parallel to the surface curvature. The survey is along a line located 5.4 mm upstream of the flap trailing edge. Points A, B, and C have been highlighted to indicate selected locations where a comparison of their velocity histograms provides some insight into the mechanics of this particular flow. The histograms for points A and C are presented in Fig. 8b and those for point B are shown in Fig. 7. For points A and B, the velocity gradient is not excessive and a simultaneity time of 10 μs results in an acceptable resolution of approximately 1 mm. Point C, however, is located only 0.51 mm from the surface where the velocity gradient is much greater. Accordingly, the spatial resolution was reduced to 0.1 mm§ by decreasing the simultaneity time to 4 μs. According to Eq. (1), the smaller value of $\bar{u}$ at this location also contributes to the improved spatial resolution. Even though this resolution is small compared to the flap boundary-layer thickness of approximately 10 mm, Sandborn[10] noted that, in regions of high mean shear, the spatial resolution is a significant factor in the accuracy attainable in a measurement of the Reynolds stresses. Subsequent to that observation,

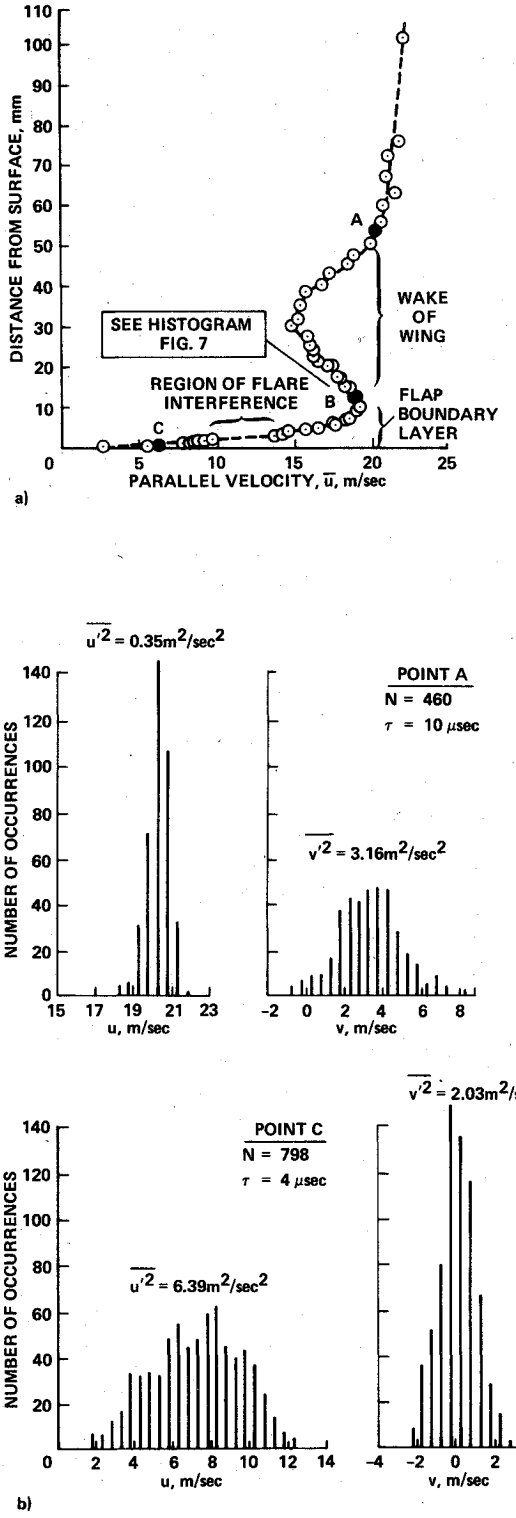

Fig. 8 Velocity data for boundary layer on flap: a) measured mean parallel velocity profile along a traverse line located 5.4 mm upstream of flap trailing edge; b) histograms for points A and C of part a. (Histogram for point B is given in Fig. 7.)

‡It is, in fact, a combination of the model installation and the constraints on optical access to the wind-tunnel test section that determined the final geometrical arrangement of the LDA.

§This is computed from Eq. (1); Fig. 4 suggests that the value may be slightly higher.

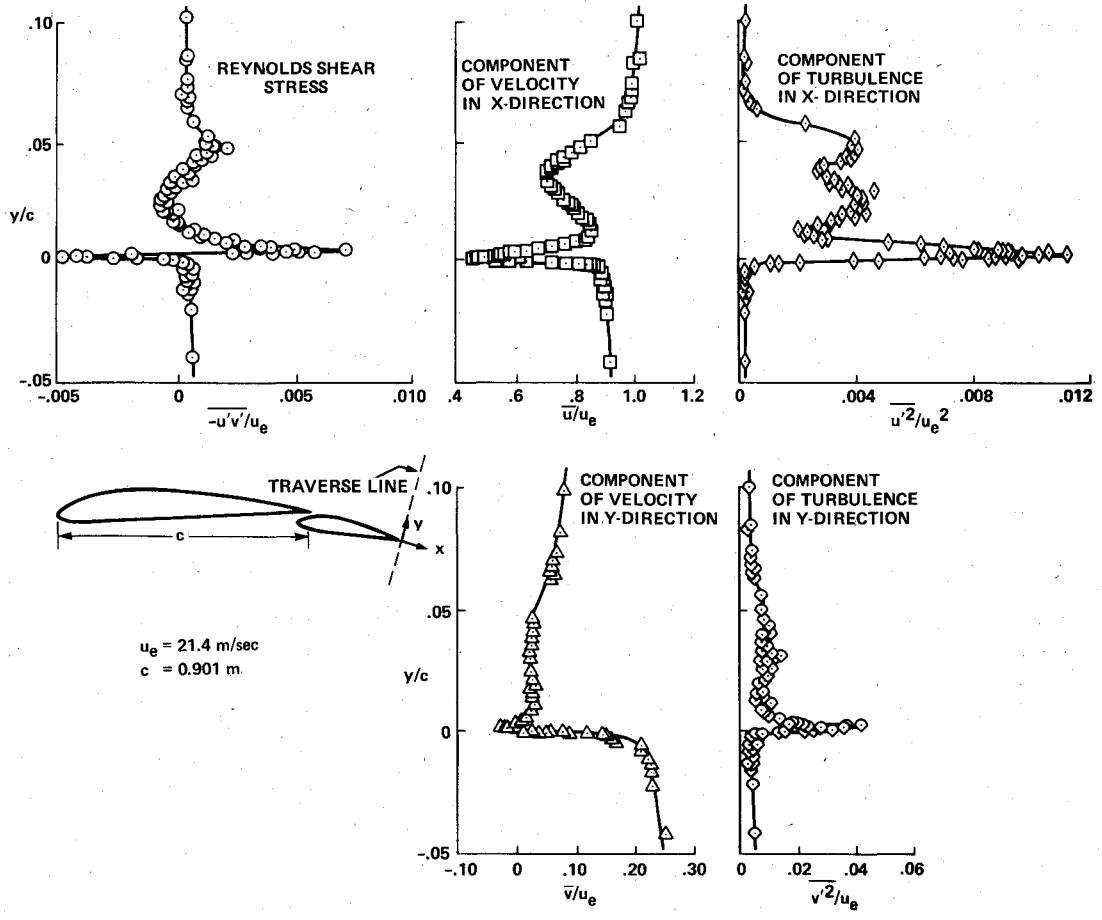

Fig. 9 Structure of the turbulent flow in the wake of a two-element airfoil showing the details measured within thin high-shear regions (non-dimensionalization based on $u_e = 21.4$ m/s and $c = 0.901$ m; y coordinate is perpendicular to the lower surface of the flap).

Karpuk and Tiederman[11] have shown that, for a linear velocity gradient, the velocity-weighted average yields a good estimate of both the mean velocity and the mean-square fluctuations at the center of the probe volume, even for a highly turbulent flow. At point C, therefore, the spatial resolution of 0.1 mm is felt to be small enough to provide this linearity.

Points A, B, and C are in regions of increasing mean shear, respectively, and as expected there is an attendant broadening of the u histogram, representing an increasing turbulent kinetic energy in the velocity component parallel to the airfoil surface. Likewise, the v histogram shows that the variance at B (3.99 m^2/s^2) is larger than the variance at A (3.61 m^2/s^2); but, in contrast, Figs. 7 and 8 show that the turbulent kinetic energy in the velocity component normal to the airfoil surface decreases between points B and C to a value (2.03 m^2/s^2) that is even lower than the level measured in the freestream (2.5 m^2/s^2). This reduction results from wall damping of the normal fluctuations due to the proximity of the flap surface. It should be emphasized that it is only through the use of the reflective surface that accurate data were obtained with the probe volume in close proximity to the surface. In fact, the cleanliness and quality of the mirror surface determine the success of the measurements within 10 mm of the surface. The boundary-layer region (Fig. 8a) where the LDA signal was overwhelmed by flare interference was probably caused by a minute deposit of foreign matter (e.g., seeding condensate), a slight coating imperfection, or a small scratch on the surface.

To further illustrate the quality of the measurements that have been made with the LDA, Fig. 9 presents a complete description of the velocity-weighted (time-averaged) turbulent wake structure at a location 13.5 mm behind the flap trailing edge. The ability to measure the detailed distribution of the Reynolds stress tensor through this wake region confirms the performance of the high-resolution LDA. This is particularly true within the flap wake, where significant excursions in the values of the mean velocity and the turbulent stresses occur within a distance of less than 5 mm. It is noteworthy that the data indicate that 1) the $\overline{u'^2}$ and $\overline{u'v'}$ components of the Reynolds stress tensor are approximately proportional to the gradient in the mean parallel velocity component $d\bar{u}/dy$, and 2) the $\overline{u'v'}$ component of the Reynolds stress is zero when the gradient of $\bar{u}$ is zero. The precision inherent in measurements such as these is of great importance to those researchers involved in the modeling of turbulent boundary layers and wakes.

Conclusion

The spatial resolution attainable using an LDA with an optical arrangement that incorporates two crossing dual-scatter channels has been shown to be effective for the long-range, remote measurement of turbulent boundary layers and thin wakes. By incorporating the concept of simultaneity into such a system, not only can the Reynolds shear stress be measured, but the effective spatial resolution can be improved even further.

A correction for velocity biasing has been included in the data reduction; it was found to be small for the mean velocity components, but significant when applied to the Reynolds stresses. There are, however, other possible biases that have not been discussed. The bias error due to gradients in the seed particle density has not been considered. Also, the analysis has not considered the validity of using the simultaneity concept [Eq. (1)] to specify the spatial resolution when the flow is highly turbulent, especially when $\overline{v'^2}$ is large and $\bar{u}$ is

small (e.g., along a wake centerline). These two problems are currently the subjects of continuing research.

Acknowledgments

The authors wish to thank Harold Yanagita for his efforts in the optical design of the LDA system, Dean Harrison for the design and fabrication of an accurate and reliable simultaneity timing interface, and Opal Lemmer for programming and debugging the user-interactive computer software.

References

[1]Orloff, K. L., Corsiglia, V. R., Biggers, J. C., and Ekstedt, T. W., "Investigating Complex Aerodynamic Flows with a Laser Velocimeter," *Proceedings of the LDA Symposium,* Technical University of Denmark, Copenhagen, 1975, pp. 624-643.

[2]Logan, S. E., "A Laser Velocimeter for Reynolds Stress and Other Turbulence Measurements," *AIAA Journal,* Vol. 10, July 1972, pp. 933-935.

[3]Boutier, A. and Lefevre, J., "Some Applications of Laser Anemometry in Wind Tunnels," *Proceedings of the LDA Symposium,* Technical University of Denmark, Copenhagen, 1975, pp. 644-662.

[4]Wiffen, M. C. and Meadows, D. M., "Two Axis, Single Particle Laser Velocimeter System for Turbulence Spectral Analysis," *Proceedings of the Second International Workshop on Laser Velocimetry,* Vol. 2, Purdue University, Lafayette, Ind., 1974, pp. 1-12.

[5]Durst, F. and Stevenson, W. H., "Influence of Gaussian Beam Properties on Laser Doppler Signals," *Applied Optics,* Vol. 18, Feb. 1979, pp. 516-524.

[6]Meyers, J. F., "Applications of Laser Velocimetry to Large Scale and Specialized Aerodynamic Tests," *TSI Quarterly,* Vol. V, Dec. 1979, pp. 5-12.

[7]Buchhave, P., George, W. K. Jr., and Lumley, J. L., "The Measurement of Turbulence with the Laser-Doppler Anemometer," *Annual Review of Fluid Mechanics,* Vol. 11, 1979, pp. 443-503.

[8]George, W. K. Jr., "Processing of Random Signals," *Proceedings of the Dynamic Flow Conference,* Baltimore, Md./Marseilles, France, Sept. 1978, pp. 757-800.

[9]Spiegel, M. R., *Probability and Statistics,* McGraw-Hill Book Co., New York, 1975.

[10]Sandborn, V. A., "Effect of Velocity Gradients on Measurements of Turbulent Shear Stress," *AIAA Journal,* Vol. 14, March 1976, pp. 400-402.

[11]Karpuk, M. E. and Tiederman, W. G., "Effect of Finite-Size Probe Volume upon Laser Doppler Anemometer Measurements," *AIAA Journal,* Vol. 14, Aug. 1976, pp. 1099-1105.